RESEARCH ARTICLE | SEPTEMBER 24 2024

Influencing the powder particle transport in high-speed laser melt injection

Special Collection: Proceedings of the International Congress of Applications of Lasers & Electro-Optics (ICALEO 2024)

Philipp Warneke ; Lucas Westermeyer ; Annika Bohlen ; Thomas Seefeld

J. Laser Appl. 36, 042023 (2024)
https://doi.org/10.2351/7.0001554

Journal of Laser Applications ARTICLE pubs.aip.org/lia/jla

Influencing the powder particle transport in high-speed laser melt injection

Cite as: J. Laser Appl. 36, 042023 (2024); doi: 10.2351/7.0001554
Submitted: 27 June 2024 · Accepted: 19 August 2024 ·
Published Online: 24 September 2024

Philipp Warneke,[1,a)] Lucas Westermeyer,[1] Annika Bohlen,[1] and Thomas Seefeld[1,2]

AFFILIATIONS

[1]BIAS - Bremer Institut für angewandte Strahltechnik GmbH, Klagenfurter Straße 5, 28359 Bremen, Germany
[2]MAPEX Center for Materials and Processes, Universität Bremen, Bibliothekstraße 1, 28359 Bremen, Germany

Note: Paper published as part of the special topic on Proceedings of the International Congress of Applications of Lasers & Electro-Optics 2024.

[a)]**Author to whom correspondence should be addressed; electronic mail:** warneke@bias.de

ABSTRACT

Using high-speed laser melt injection (HSLMI), it is possible to generate wear-resistant metal matrix composite (MMC) surfaces on tools with great productivity. Since high laser intensities are required for reaching high process speeds, strong interactions can occur between powder particles and the laser beam. In order to reduce the interaction time and gain a better understanding of the role of particle transport in the HSLMI process, trajectories of spherical fused tungsten carbide (SFTC) particles were analyzed using high-speed imaging. The trajectories were divided into a path outside the laser beam and a path inside the laser beam. The identified interaction mechanisms were particle deformations, the formation of agglomerates, and particle disintegration. The volume flow rate of the feeding gas was found to have a decisive influence on the travel time of the particles, whereas the powder feed rate and the working distance of the powder nozzle only had a minor influence. Consequently, an increased volume flow rate led to a significant reduction of interactions between SFTC particles and the laser beam.

Key words: laser melt injection, metal matrix composite, high-speed imaging

I. INTRODUCTION

Laser melt injection is an established technology for generating wear-resistant metal matrix composite (MMC) layers on metallic components. Although the setup is similar to laser cladding and laser alloying, the principle of the process is fundamentally different. The powder is melted to form coatings in cladding and alloying, whereas the powder particles are supposed to remain solid and reinforce the metallic substrate in laser melt injection as shown in Fig. 1. In addition to this single-stage process, it is also possible to use a two-stage process in which hard particles are deposited on the substrate with a binder before the surface is irradiated by the laser beam.[1] The hard material can be selected depending on the wear protection requirements. In general, a high melting temperature of the material is necessary to avoid melting the hard particles in the laser beam. The hardness of the hard materials used in laser melt injection is usually between 1200 and 3500 HV.[2,3] This makes laser melt injection particularly interesting when having increased wear protection requirements.

Over the last years, laser melt injection has been continuously developed with regard to the resulting properties of the MMC layer. Substantial research has focused on processing various substrate/hard material combinations and process optimizations. For example, the hard particle distribution within the MMC layer could be controlled by applying a magnetic field[4] or by using the keyhole welding effect.[5] The hard particle distribution could also be influenced by using specific scanning patterns.[6] By additionally controlling the melt pool temperature, very homogeneous layer thicknesses could be generated. Furthermore, it was investigated how the highest possible hard particle content can be achieved in the MMC layer.[3] It was found that hard particle damage and the formation of agglomerates can occur depending on the energy per unit length and the powder mass per unit length, which limits the

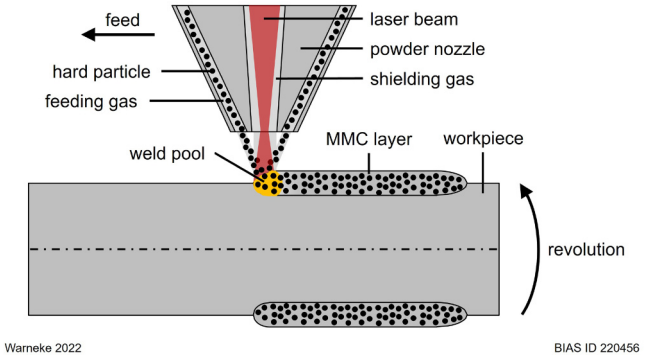

FIG. 1. Schematic diagram of laser melt injection.

hard particle content. It was shown that a high hard particle content can reduce adhesive wear in deep-drawing tools.[7] In addition, hard particle agglomerates could be generated intentionally in a second processing step after laser melt injection in order to generate particularly high wear resistance in tool zones exposed to extremely high stress.[8]

Compared to laser cladding, the process speed in laser melt injection is usually significantly lower. A fundamental disadvantage is the need to melt a larger volume of the substrate in order to ensure adequate distribution of the hard particles. Typically, the process speeds are below 1 m/min and the laser intensities below 20 kW/cm^2, resulting in relatively low productivity.[3,9] To overcome this drawback, high-speed laser melt injection (HSLMI) was developed for reaching process speeds up to 100 m/min.[10] It was already shown that HSLMI can be used to reinforce tools made of steel and copper alloys, such as skin-pass rolls and pressure die casting pistons.[11,12] However, since high laser intensities are required for reaching high process speeds, strong interactions can occur between hard particles and the laser beam, leading to undesirable particle deformations. Hence, there is a need for a fundamental understanding of the hard particle transport in HSLMI.

During the powder particle transport in laser processes, the geometries of the laser beam and of the powder jet are among the most important influencing factors.[13] The powder jet geometry depends on the powder nozzle, especially on the injector diameter and the working distance of the nozzle,[14] as well as on process parameters such as the volume flow rate of the feeding gas and the powder particle size.[15,16] In addition to the powder jet geometry, the particle's travel velocity has a decisive impact on laser-powder-interactions since it affects the time a particle spends in the laser beam. It was found that the travel velocity increases with the volume flow rate of the feeding gas and that it decreases as the particle size increases.[16,17] When increasing the powder feed rate from 5 to 25 g/min, a slight decrease in travel velocity was identified.[18] However, the drop in travel velocity decreased with increasing powder feed rate. For travel velocities below 2 m/s^{-1}, an increase in travel velocity was found over the distance between the nozzle outlet and the powder focus.[19] Usually, the velocity of the feeding gas is higher than the particle's travel velocity.[17] Laser-powder-interactions have already been investigated for laser cladding, especially for high-speed cladding, where rapid melting of powder particles in the laser beam is desired. It was determined that small particles are heated significantly faster in the laser beam than large particles.[20] Furthermore, it was found that shadowing effects occur at high powder feed rates.[21] By calculating the heating of powder particles, it was determined that the shadowing effects increase with the powder feed rate and lead to a drop in the proportion of liquid particles.[18]

In summary, laser-powder-interactions are of great interest for HSLMI since high process speeds can only be reached with high laser intensities. While strong interactions are often desirable for rapid melting of powder particles in laser cladding, the melting of powder particles during laser melt injection is undesired. Although initial studies of interactions during particle transport have already been carried out for laser cladding, laser-powder-interactions in HSLMI are not yet sufficiently understood. Hence, this paper focuses on the hard particle transport from the powder nozzle to the melt pool and the interaction mechanisms occurring during the transport. Moreover, understanding the hard particle transport is a necessary step for investigating the particle incorporation in the melt pool.

II. EXPERIMENTAL METHODS

A. Materials

The cold working steel 1.2362 (X63CrMoV5-1) was used as the substrate material. The cylindrical workpieces had a diameter of 80 mm. Table I gives an overview of the most important material properties. As the reinforcing phase, spherical fused tungsten carbide (SFTC) particles featuring a grain size of 45 to 106 μm and a hardness of 2700 to 3500 HV 0.1[23] were used. Fused tungsten carbide is a eutectic material of 20 to 27 % WC and 73 to 80 % W_2C.[25] Figure 2 shows cross sections of the SFTC particles in their initial states. Some of the particles had pores or breakouts.

B. High-speed laser melt injection

For HSLMI, a 12 kW disk laser (Trumpf TruDisk 12 002) with a wavelength of 1030 nm was used. An optical fiber with a diameter of 200 μm and a processing optic (Trumpf BEO D70) were used for beam guidance and shaping. The processing optic was moved using a six-axis robot (Reis) parallel to the rotational axis of the workpiece. The workpiece was positioned 15 mm below the laser focus,

TABLE I. Materials used for HSLMI.

	1.2362 (X63CrMoV5-1)[22]	Fused tungsten carbide[23,24]
Chemical composition in wt.-%	C: 0.6…0.65, Si: 1…1.2, Mn: 0.3…0.5, Cr: 5…5.5, Mo: 1…1.3, V: 0.25…0.35, Fe: balance	C: 3.8, W: balance
Melting point in °C	1480 (estimated from iron carbon diagram)	2735
Hardness	225 HB (annealed)	2700…3500 HV

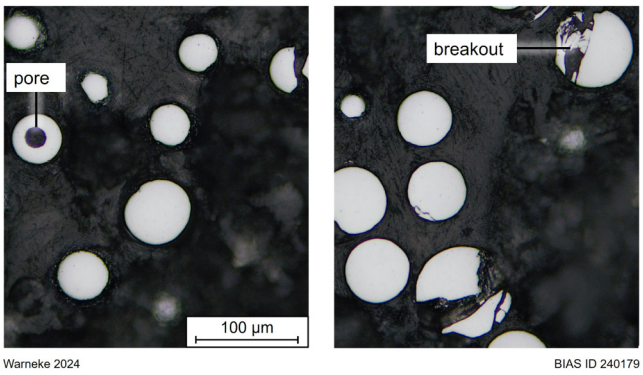

FIG. 2. Cross sections of SFTC particles in their initial states.

obtaining a laser spot with a diameter of 2 mm on the surface. A three-jet powder nozzle (Ixun) with a working distance of 16 mm was used. The SFTC particles were transported to the powder nozzle by a powder feeder (GTV PF 2/2). Argon was used as both feeding gas and shielding gas. The overlapping degree was set to 50 %. An overview of the used parameters for HSLMI is given in Table II.

C. High-speed imaging and analysis

To analyze hard particle transport, a high-speed camera (iX Cameras i-SPEED 7) was used in combination with an illumination laser (Cavilux HF) featuring a wavelength of 810 nm. The illumination laser made it possible to clearly visualize the hard particles by illuminating them at a specific wavelength and filtering out the process emissions of the residual spectrum. In addition, the illumination laser enabled a very high frame rate of 200 kHz. The pulse duration of the illumination laser was 0.09 μs.

For measuring the travel velocity of hard particles, the captured images were processed with MATLAB and IMAGEJ. First, the images were inverted and the static background was removed, producing bright particles on an all-black background. Second, the particles were tracked with a linear motion tracker using a Kalman filter. For investigating the influence of the volume flow rate and the powder feed rate on the travel velocity, the average velocity over the distance between the powder nozzle and the powder focus was determined. For analyzing the travel velocity over the working distance of the nozzle, the images were divided into 16 strips with a height of 1 mm, and the particle's average velocity within each strip was determined.

TABLE II. Parameters for HSLMI.

Laser power in kW	6.7
Process speed in m/min	50
Powder feet rate in g/min	10…90
Feeding gas volume flow rate in L/min	5…20
Shielding gas volume flow rate in L/min	8

D. Measuring the feeding gas velocity

The feeding gas velocity was determined using the principle of differential pressure. A Prandtl tube and a differential pressure sensor (Testo 510) were used. The Prandtl tube was adjusted coaxially to one of the three powder injectors of the powder nozzle and moved in steps of 1 mm in the direction of gas flow. The measurements were carried out without powder. The feeding gas velocity v_F was derived from

$$v_F = \sqrt{\frac{2\Delta p}{\rho}}, \tag{1}$$

where Δp is the pressure difference between the inner and outer vents of the Prandtl tube and ρ is the density of the feeding gas.[26]

E. Metallographic preperation and analysis

MMC samples were cut from cylindrical workpieces using wire electric discharge machining (Mitsubishi MV 12 009 V). Cross sections were prepared by hot mounting (Struers LevoFast) and grinding up to a grit of P1200. Two polishing steps were carried out, one with a 3 μm diamond suspension and one with a 0.25 μm silicon oxide suspension. A light microscope (Zeiss AX10) was used for taking images of the cross sections.

The measurement of circularity C of SFTC particles was carried out on cross sections. It was determined in two ways: on the one hand, via the ratio of the diameter of the largest inner circle and the smallest enclosing circle, d_I to d_E, and on the other hand, via the ratio of the cross-sectional area of the particle A_{SFTC} to the perimeter P_{SFTC}. In each case, the mean value was determined from several individual measurements:

$$C_1 = \frac{1}{n}\sum_{i=1}^{n}\frac{d_{I,i}}{d_{E,i}}, \tag{2}$$

$$C_2 = \frac{1}{n}\sum_{i=1}^{n}\frac{4\pi A_{SFTC,i}}{P^2_{SFTC,i}}. \tag{3}$$

III. MODELING

A. Hard particle transport and incorporation

A simplified model for hard particle transport and incorporation was developed for laser melt injection. It was assumed that the particles move on straight-line trajectories from the powder nozzle to the melt pool, see Fig. 3. The transport and incorporation path of a particle s_φ within a single powder jet depends on a divergence angle φ. If $\varphi = 0$, the hard particle travels axially to the powder jet and hits the center of the melt pool. As a simplification, it is assumed that the melt pool width corresponds to the laser spot diameter d_L. The transport and incorporation paths s_φ can be divided into a transport path outside the laser beam $s_{\varphi,F}$, a transport path within the laser beam $s_{\varphi,L}$, and an incorporation path $s_{\varphi,I}$. The total transport path $s_{\varphi,FL}$ correlates with the working distance of the powder nozzle a via

$$a = s_{\varphi,FL} \cdot \cos(\gamma - \varphi). \tag{4}$$

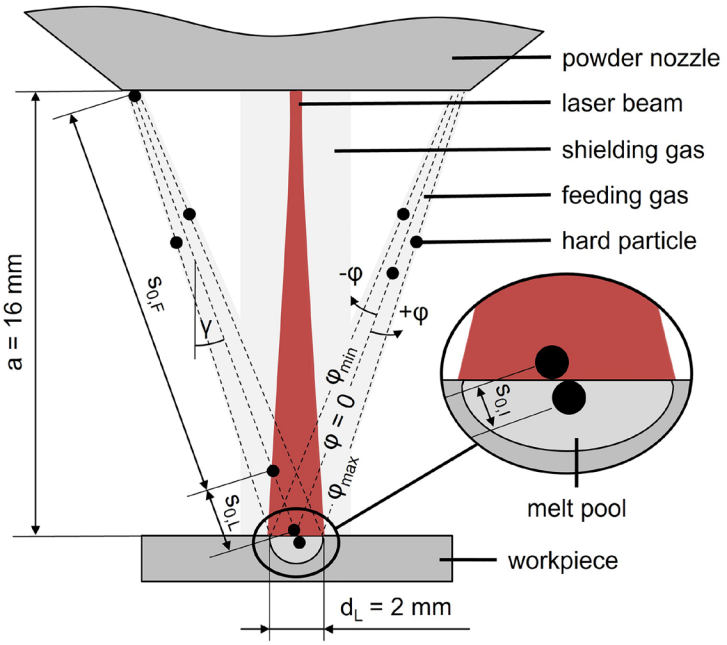

FIG. 3. Model for hard particle transport and incorporation in laser melt injection.

γ is the angle between the transport path $s_{\varphi,FL}$ and the vertical. A mean velocity can be determined for the total transport path from the powder nozzle to the impact on the melt pool surface:

$$\overline{v}_{\varphi,FL} = \frac{s_{\varphi,F} + s_{\varphi,L}}{t_{\varphi,F} + t_{\varphi,L}} = \frac{s_{\varphi,FL}}{t_{\varphi,FL}}. \tag{5}$$

The incorporation path $s_{\varphi,I}$ is defined as the distance that a particle travels from the first contact with the surface of the melt pool until it is fully incorporated in the melt pool. Accordingly, the overall interaction time with the laser beam is

$$t_{int} = t_{\varphi,L} + t_{\varphi,I}. \tag{6}$$

$\overline{v}_{\varphi,FL}$ depends on the initial velocity of a particle at the powder nozzle's exit $v_{initial,1}$, on the force F_F applied to a particle by the feeding gas volume flow $\dot{V}_F$ and on the weight force F_G:

$$\overline{v}_{\varphi,FL} = f(v_{initial,1}, F_F, F_G). \tag{7}$$

The flow force of the feeding gas F_F is calculated as follows:

$$F_F = \frac{1}{2} \cdot c_W \cdot A_{SFTC} \cdot \rho_F \cdot (v_F - \overline{v}_{\varphi,FL})^2. \tag{8}$$

A_{SFTC} is the frontal area of an SFTC particle, ρ_F is the density of the feeding gas, and v_F is the gas velocity. The drag coefficient c_W for a sphere is between 0.2 and 0.4.[27]

B. Critical interaction time

In laser melt injection, melting of hard particles is undesirable. A hard particle melts as soon as the energy absorbed by a particle E_A is equal to the energy required to melt the particle volume E_{SFTC}:

$$E_{SFTC} = E_A. \tag{9}$$

Heat loss due to convection and radiation is neglected due to a short interaction time t_{Int}. The energy for melting the particle volume E_{SFTC} can be determined as follows if the enthalpy of fusion is neglected:

$$E_{SFTC} = V_{SFTC} \cdot \rho_{SFTC} \cdot c_{p,SFTC} \cdot (T_M - T_0). \tag{10}$$

A perfect spherical geometry is assumed to calculate the particle volume V_{SFTC}. The density is assumed to be $\rho_{SFTC} = 15.95\ \mathrm{g/cm^3}$[24] and the specific heat capacity is assumed to be that of tungsten carbide at the mean temperature 1380 °C, $c_{p,SFTC} = 0.31\ \mathrm{kJ/kg\ K}$.[28] The melting temperature is $T_M = 2735\ ^\circ\mathrm{C}$ and the room temperature is $T_0 = 25\ ^\circ\mathrm{C}$.[24] The absorbed energy E_A can be calculated as follows:

$$E_A = \frac{P_L}{A_L} \cdot \eta_A \cdot A_{SFTC} \cdot t_{int}. \tag{11}$$

η_A is the absorption efficiency. The laser power is $P_L = 6.7\ \mathrm{kW}$ and the area of the laser spot $A_L = \frac{\pi}{4} d_L^2$ with the laser spot diameter $d_L = 2\ \mathrm{mm}$. For simplification, a homogeneous intensity

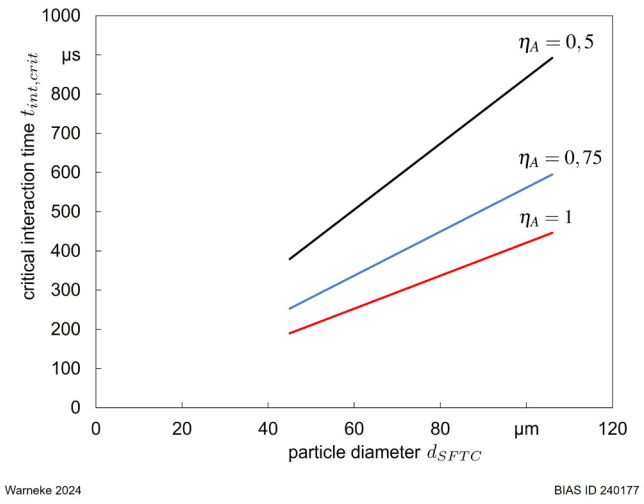

FIG. 4. Influence of the particle diameter d_{SFTC} and the absorption efficiency η_A on the critical interaction time $t_{int,crit}$.

distribution over the beam radius is assumed. After inserting Eqs. (10) and (11) into Eq. (9), the critical interaction time $t_{int,crit}$ can be determined:

$$t_{int,crit} = \frac{V_{SFTC} \cdot \rho_{SFTC} \cdot c_{p,SFTC} \cdot (T_M - T_0)}{\frac{P_L}{A_L} \cdot \eta_A \cdot A_{SFTC}}. \quad (12)$$

The critical interaction time $t_{int,crit}$ depends largely on the particle size and the absorption efficiency η_A, see Fig. 4. It increases linearly with the particle diameter d_{SFTC} due to the change in the volume to surface ratio. The real absorption in hard particles during laser melt injection is complex, as—in addition to the direct absorption in the laser beam—reflected radiation from the melt pool surface or the surface of other particles can also be absorbed by the hard particles. On the other hand, there is mutual shadowing of the particles, which has a particular effect on particles on the outer transport path $s_{a,L}$. As a result, the laser power actually absorbed by a particle depends on the individual trajectory. Typical assumptions for the absorption efficiency of powder particles in a laser beam are between $\eta_A = 0.5$[21] and $\eta_A = 1$.[29]

IV. RESULTS

A. Off-process investigation of the particle transport

Hard particle transport was analyzed using high-speed videos. Figure 5 shows the three individual powder jets of the nozzle. It was investigated how the mean travel velocity $\overline{v}_{\varphi,FL}$ depends on the volume flow rate of the feeding gas $\dot{V}_F$ and on the powder feed rate $\dot{m}_P$. Figure 6 shows a linear correlation between the mean travel velocity $\overline{v}_{\varphi,FL}$ and the volume flow rate $\dot{V}_F$, whereas the powder feed rate $\dot{m}_P$ had no significant influence on the mean travel velocity $\overline{v}_{\varphi,FL}$. Therefore, the volume flow rate $\dot{V}_F$ can be identified as a significant factor influencing the particle velocity.

Furthermore, the correlation between the travel velocity $v_{\varphi,FL}$ and the working distance of the powder nozzle a was investigated for different volume flow rates of the feeding gas $\dot{V}_F$, see Fig. 7. It was found that the travel velocity $v_{\varphi,FL}$ decreases only very slightly for all investigated volume flow rates $\dot{V}_F$ when increasing the working distance a. Due to the slight change in the travel velocity $v_{\varphi,FL}$ over the working distance a, it could be found that the forces F_F and F_G play a minor role during the travel distance $s_{\varphi,FL}$ and that

$$v_{initial,1} \approx v_{initial,2}, \quad (13)$$

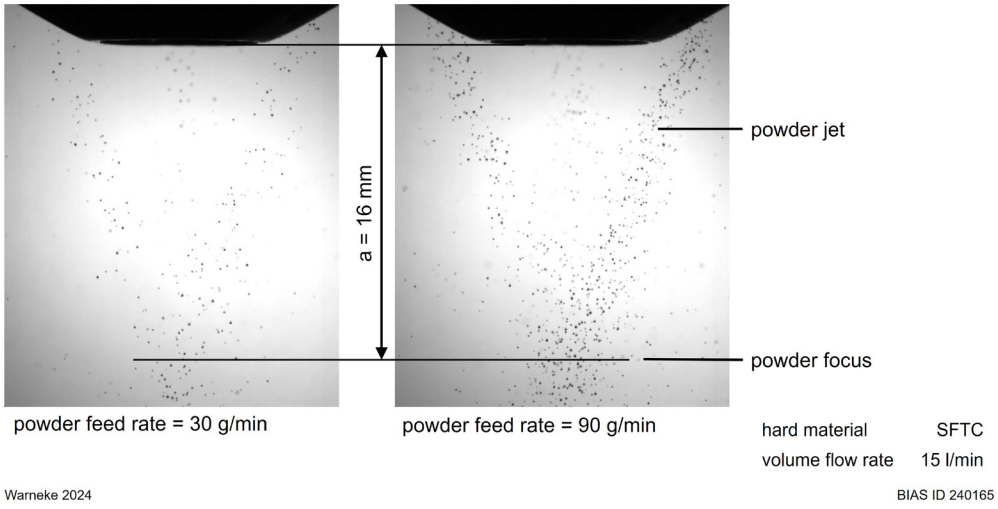

FIG. 5. Powder jets of a 3-jet-nozzle. Frames from high-speed videos.

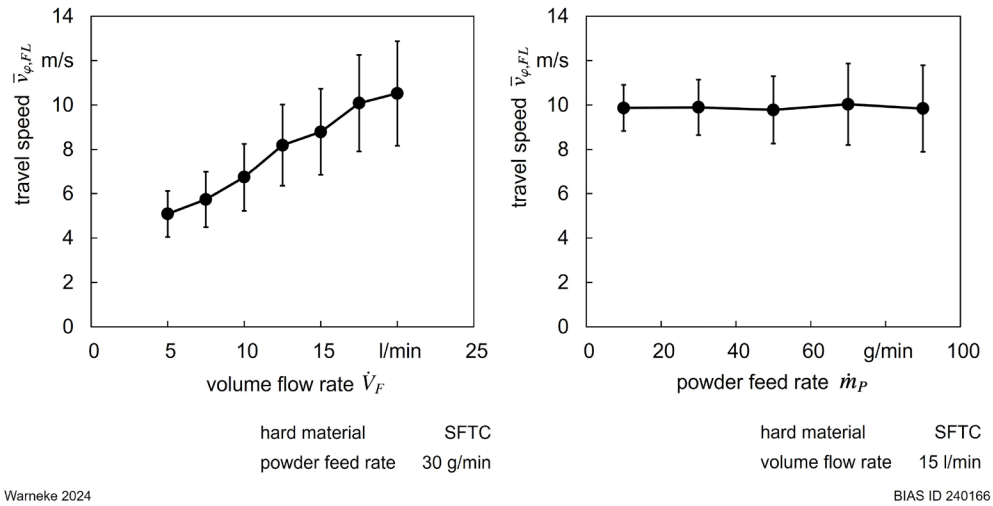

FIG. 6. Travel speed $\bar{v}_{\varphi,FL}$ as a function of the volume flow rate $\dot{V}_F$ and the powder feed rate $\dot{m}_P$.

when $v_{initial,2}$ is the travel velocity at the particle's arrival at the melt pool. The velocity of the feeding gas v_F was significantly higher than the travel velocity of the hard particles $\bar{v}_{\varphi,FL}$ for all investigated volume flow rates $\dot{V}_F$, see Fig. 8. There was a linear correlation between the feeding gas velocity v_F and the volume flow rate $\dot{V}_F$. The feeding gas velocity v_F decreased when increasing the working distance a. Above a working distance a of 10 mm, the feeding gas velocity v_F dropped progressively.

However, since the travel velocity $v_{\varphi,FL}$ changed only slightly over the working distance a, the travel time in the laser beam $t_{0,L}$ could be calculated using the mean travel velocity $\bar{v}_{\varphi,FL}$, see Fig. 9. Due to the linear correlation between the volume flow rate $\dot{V}_F$ and the mean travel velocity $\bar{v}_{\varphi,FL}$, a linear correlation was also found between the volume flow rate $\dot{V}_F$ and the travel time in the laser beam $t_{0,L}$. For large and average-sized particles with a diameter d_{SFTC} between 75.5 and 106 μm and an absorption efficiency η_A of 50 %, the travel time $t_{0,L}$ was below the critical interaction time $t_{int,crit}$ for all investigated volume flow rates $\dot{V}_F$. When applying a volume flow rate $\dot{V}_F$ in the range between 12.5 and 20 L/min, the travel time $t_{0,L}$ of very small particles with a diameter d_{SFTC} of 45 μm was also below the critical interaction time $t_{int,crit}$.

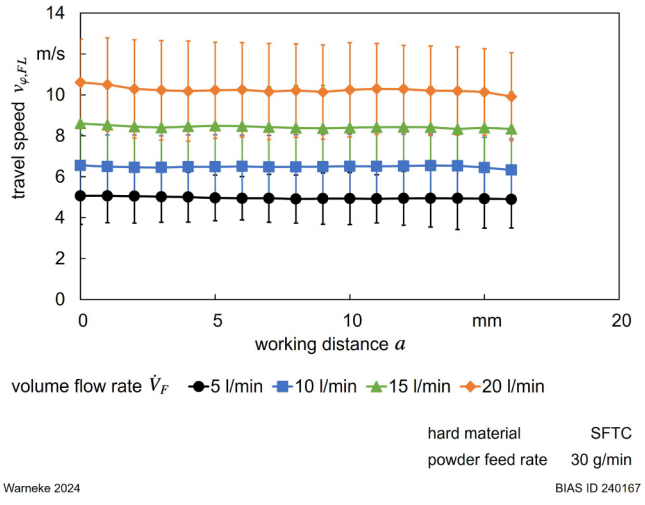

FIG. 7. Travel speed $\bar{v}_{\varphi,FL}$ as a function of the working distance of the powder nozzle a. Each data point represents an average of travel speeds $v_{\varphi,FL}$ at a working distance of $a \pm 0.5$ mm.

B. In-process investigation of the particle transport

For analyzing the hard particle transport during HSLMI, high-speed videos with a high frame rate of 200 kHz were used. The high frame rates made it possible to observe the mechanisms occurring during hard particle transport immediately before reaching the melt pool. Due to a comparatively long travel time in the laser beam $t_{\varphi,L}$, strong interactions were observed much more frequently at low volume flow rates $\dot{V}_F$ than at high volume flow rates. These included deformations and agglomerations of particles that had already formed before reaching the melt pool. Figure 10(a) shows that an originally spherical particle has partially melted and the spin of the particle has caused an increasing deformation. A collision of partially melted particles led to the formation of agglomerates, see Fig. 10(b). Furthermore, at low volume flow rates $\dot{V}_F$, some particles disintegrated explosively, see Fig. 10(c). First, the volume of the observed particle increased drastically within 40 μs and, second, the particle disintegrates into various fragments. Afterward, some of these fragments entered the melt pool.

The strong interactions shown in Fig. 10 are caused by the high laser intensity required for high-speed processing. The amount of particle deformations and other undesirable

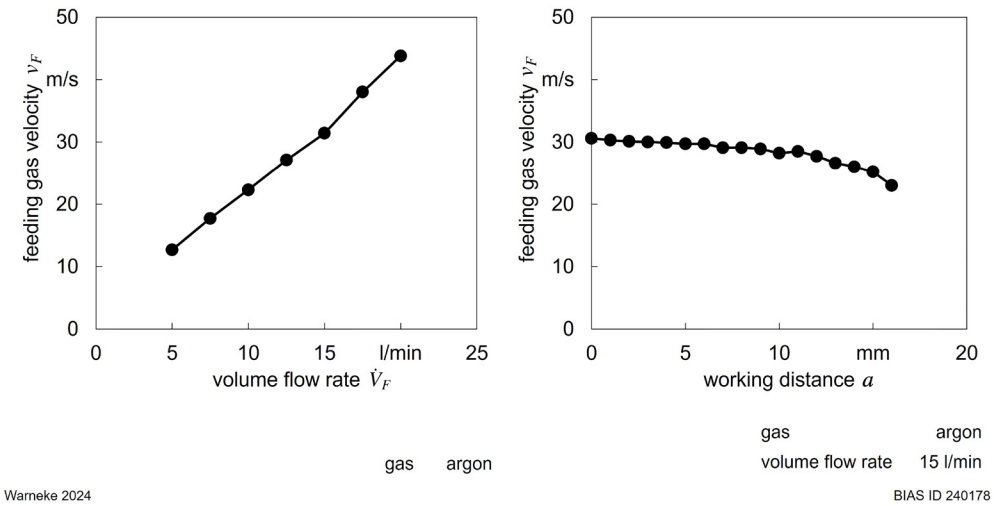

FIG. 8. Feeding gas velocity v_F as a function of the volume flow rate $\dot{V}_F$ and the working distance a.

mechanisms, which result in a change in geometry of the particles, could be clearly reduced by using an increased volume flow rate $\dot{V}_F$ of 15 L/min and a resulting mean travel velocity of the particles $\overline{v}_{\varphi,FL}$ of 9 m/s. Figure 11 shows cross sections of MMC-layers that were produced with different volume flow rates $\dot{V}_F$. The MMC coatings produced with a volume flow rate $\dot{V}_F$ of 5 and 10 L/min featured a significantly higher proportion of deformed particles and agglomerates. In addition, some breakouts were found. Significantly better results were achieved with an increased volume flow rate $\dot{V}_F$ of 15 and 20 L/min. The MMC-layers were more homogeneous and had fewer deformations and agglomerates. The degree of deformation of the particles was analyzed using

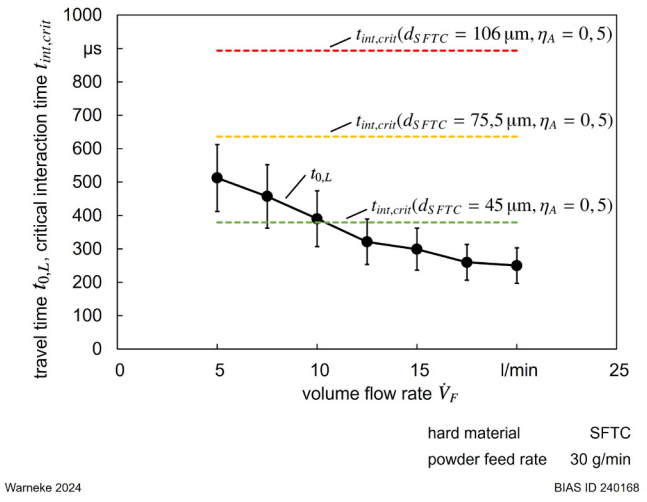

FIG. 9. Calculated travel time $t_{0,L}$ as a function of the volume flow rate $\dot{V}_F$.

circularity measurements on cross sections, see Fig. 12. It was found that the circularity of the particles C_1 and C_2 increased continuously with the feeding gas volume flow rate $\dot{V}_F$. No significant improvement in circularity could be found with the use of SFTC particles with a large diameter d_{SFTC} of 90–106 μm.

V. DISCUSSION

Whereas heating the powder particles to melting temperature before hitting the melt pool can be advantageous in laser cladding, it is undesirable in laser melt injection where this means exceeding the limit of the process. At low process speeds associated with low laser intensities, melting of hard particles does not usually occur due to the comparatively high melting temperatures of ceramic hard materials that are frequently used for laser melt injection. However, a significantly higher laser intensity of 212 kW/cm^2 is required for high-speed processing, which means that even hard particles featuring a high melting temperature can melt in the laser beam. Therefore, the interaction time in the laser beam t_{Int} and particle heating are particularly important in HSLMI.

The experimental results show that the travel velocity $\overline{v}_{FL}$, which has a decisive influence on the interaction time in the laser beam t_{Int}, can be adjusted very well via the feeding gas volume flow rate $\dot{V}_F$. The correlation between the feeding gas volume flow rate $\dot{V}_F$ and the travel velocity $\overline{v}_{FL}$ largely corresponds to the findings of Li *et al.* and Yao *et al.*[16,17] The powder feed rate $\dot{m}_P$ and the working distance a, on the other hand, only have a minor influence on the travel velocity $\overline{v}_{\varphi,FL}$. The low interaction of these parameters offers the advantage that the travel velocity $\overline{v}_{\varphi,FL}$ can be set via the feeding gas volume flow rate $\dot{V}_F$ mostly independently from other process parameters. In contrast, the results of *Schopphoven* show a decrease in the particle's travel velocity with increasing powder feed rate.[18] However, it needs to be considered that the experiments of *Schopphoven* were conducted with significantly smaller feeding gas volume flow rates (between 4 and 6 L/min). A small feeding gas volume flow rate results in a

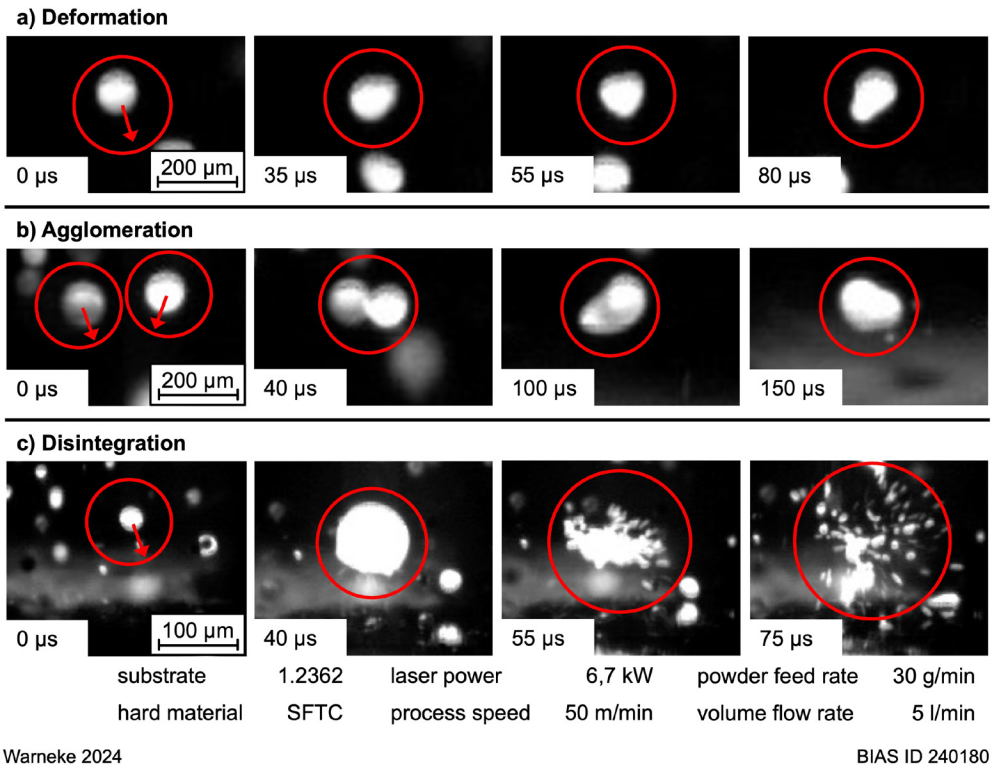

FIG. 10. Interaction mechanisms during hard particle transport. Frames from high-speed videos.

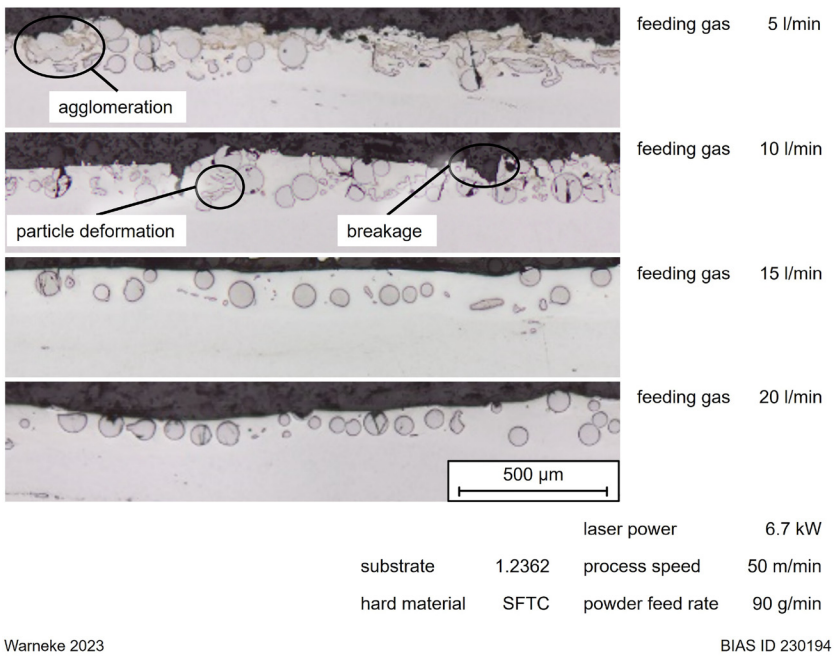

FIG. 11. Influence of the volume flow rate $\dot{V}_F$ on the MMC layer. Cross sections.

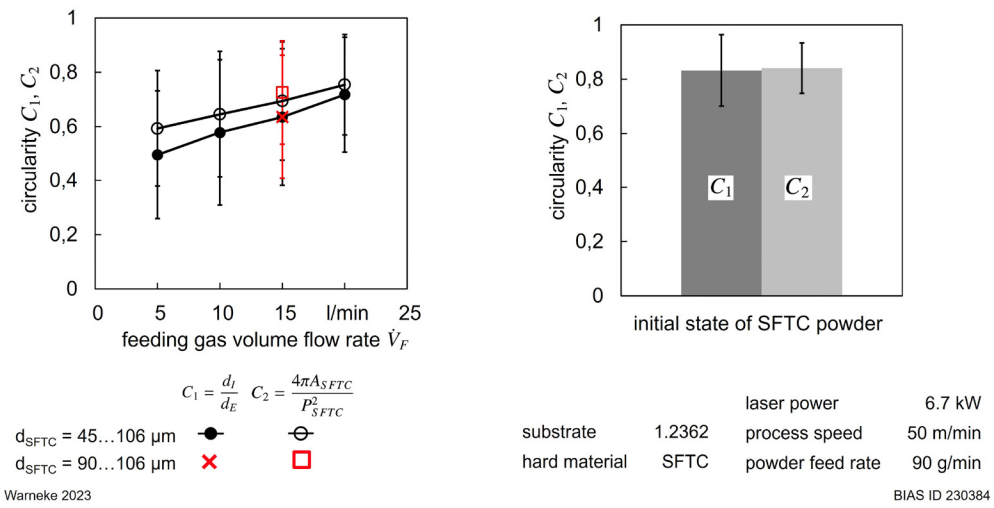

FIG. 12. Circularity C of SFTC particles in cross sections.

comparatively low powder density in the powder jet. For HSLMI, a high feeding gas volume flow rate is necessary which results in a comparatively low powder density in the powder jets. Furthermore, Wang *et al.* found a decrease in the particle's travel velocity with increasing working distance.[19] However, the travel velocity in the experiments of Wang *et al.* was significantly smaller. The effect of gravity on the travel velocity is larger when the travel velocity at the nozzle outlet is smaller since the law of conservation of energy (neglecting the flow force of the feeding gas) is given by

$$\frac{1}{2} \cdot m_{SFTC} \cdot v_{initial,2}^2 = \frac{1}{2} \cdot m_{SFTC} \cdot v_{initial,1}^2 + m_{SFTC} \cdot g \cdot a, \tag{14}$$

resulting in

$$v_{initial,2} = \sqrt{v_{initial,1}^2 + 2 \cdot m_{SFTC} \cdot g \cdot a}. \tag{15}$$

m_{SFTC} is the mass of an SFTC particle, g is the gravity, and a is the working distance of the powder nozzle.

Although it was found that particle deformations can be significantly reduced by high volume flow rates $\dot{V}_F$ on average, some particles were deformed even at high volume flow rates $\dot{V}_F$. This can be explained by different trajectories of the particles leading to different transport distances in the laser beam $s_{\varphi,L}$. The model presented in this paper shows that heating of the hard particles by the laser beam during the transport in the gas flow depends strongly on the travel velocity $\overline{v}_{\varphi,FL}$ and the divergence angle of the transport path φ. The divergence angle φ determines the transport distance $s_{\varphi,L}$, and therefore, together with the mean travel velocity $\overline{v}_{\varphi,FL}$, the interaction time of a particle in the laser beam. Furthermore, the number of potential particles that travel over a particular particle and temporarily shadow it from the laser beam depends on the individual trajectory, which can have an effect on the actual laser power absorbed by a particle. The shadowing effect of powder particles is a typical phenomenon in laser cladding and laser melt injection.[21,18] Based on these relations, it can be assumed that the innermost transport path s_{i_L} is the most critical and the outermost transport path $s_{a,L}$ is the optimum with regard to the interaction with the laser beam. In addition, there are always particles that spend significantly more time in the laser beam, e.g., particles that first bounce off the solid workpiece and then travel through the laser beam at reduced speed.

With the help of high-speed videos with high frame rates, it was possible to observe and analyze the mechanisms during the hard particle transport in HSLMI for the first time. Particle deformation, agglomeration, and disintegration were identified as mechanisms in the hard particle transport inside the laser beam. Deformations can be increased by forces acting on a particle after the melting temperature has been reached. These include centrifugal forces due to a particle spin; see Fig. 10(a). Furthermore, they include impact forces that occur when a particle hits the surface of the molten pool or collides with another particle. In case of a collision between two molten particles, the formation of agglomerates is likely. The strong increase in a particle's volume shown in Fig. 10(c) before the disintegration of a particle indicates the expansion of a gas pore within the particle. In the initial state of the SFTC powder, some pores could be identified; see Fig. 2. As the temperature of a particle increases, the viscosity of the molten particle decreases, so that a sudden expansion of the gas pore becomes possible. In addition, the expansion of an SFTC particle leads to a significant increase in surface area irradiated by the laser, which can cause a further increase in absorption.

VI. CONCLUSIONS

It was shown that high laser intensities, which are necessary for high-speed laser melt injection (HSLMI), lead to strong

interactions between hard particles and the laser beam. Three different mechanisms were observed during the transport of the particles through the laser beam: particle deformation, particle agglomeration, and particle disintegration. The travel velocity of the hard particles was identified as a decisive parameter for achieving high process speeds for laser melt injection since it influences the interaction time of the particles in the laser beam. The travel velocity is mainly influenced by the feeding gas volume flow rate. The powder feed rate and the working distance of the powder nozzle, on the other hand, play a minor role. By increasing the travel velocity, the interactions can be significantly reduced so that homogeneous metal matrix composite (MMC) layers can be generated.

ACKNOWLEDGMENTS

The authors gratefully acknowledge the support of this work by Deutsche Forschungsgemeinschaft (DFG) within the project *Effect of wetting on the incorporation behavior of powder particles in laser melt injection at high processing speed* (no. 495532447).

AUTHOR DECLARATIONS

Conflict of Interest

The authors have no conflicts to disclose.

Author Contributions

Philipp Warneke: Conceptualization (lead); Data curation (equal); Investigation (equal); Methodology (lead); Visualization (lead); Writing – original draft (lead). **Lucas Westermeyer:** Data curation (equal); Investigation (equal). **Annika Bohlen:** Methodology (supporting); Supervision (supporting). **Thomas Seefeld:** Conceptualization (supporting); Supervision (lead); Writing – review & editing (lead).

REFERENCES

[1]K. Hilgenberg, F. Spranger, and M. Bachmann, "Localized laser dispersing of titanium-di-boride with pulsed fiber laser," in *Proceedings of the International Congress on Applications of Lasers and Electro-Optics (ICALEO)* (Laser Institute of America, Orlando, FL, 2017).
[2]M. Deutschmann, "Lasergestützte Herstellung von Keramik-Stahl-Werkstoffverbundschichten für Werkzeuge der Blechumformung," Dissertation (Gottfried Wilhelm Leibniz Universität Hannover, Hannover, 2007).
[3]H. Freiße, "Hartpartikelverstärkte Oberfläche für das Trockentiefziehen eines hochlegierten Stahls," Dissertation (Universität Bremen, Bremen, 2020).
[4]L. Wang, J. Yao, Y. Hu, Q. Zhang, Z. Sun, and R. Liu, "Influence of electric-magnetic compound field on the WC particles distribution in laser melt injection," Surf. Coat. Technol. **315**, 32–43 (2017).
[5]F. Vollertsen, G. Habedank, and K. Partes, "Maßgeschneiderte tribologie durch laseroberflächenbehandlung," Materialwiss. Werkstofftech. **39**(1), 88–92 (2008).
[6]A. Fedorov Kukk, H. Freiße, A. Bohlen, and F. Vollertsen, "Laser melt injection of hard particles with beam wobbling for wear protection of micro-injection molding tools," in *Proceedings of the 10th Lasers in Manufacturing Conference* (Wissenschaftliche Gesellschaft Lasertechnik, München, 2019).
[7]H. Freiße, A. Ditsche, and T. Seefeld, "Reducing adhesive wear in dry deep drawing of high-alloy steels by using MMC tool," Manuf. Rev. **6**, 1–6 (2019).
[8]A. Ditsche and T. Seefeld, "Local laser particle fusion: Fusing of hard particles for the reduction of high contact pressures in mmc tool surfaces," JOM **72**(7), 2488–2496 (2020).
[9]M. Student, H. Pokhmurska, K. Zadorozhna, A. Dzyubyk, and I. Khomych, "Structure and wear resistance of aluminium alloys coated with surface layer laser-modified by silicon carbide," Ukrainian J. Mech. Eng. Mater. Sci. **4**(1), 49–57 (2018).
[10]P. Warneke, A. Bohlen, and T. Seefeld, "Improving the wear resistance of copper tools for pressure die casting by laser melt injection," Prod. Eng. **17**, 453–462 (2023).
[11]P. Warneke, A. Bohlen, and T. Seefeld, "Texturing skin-pass rolls by high-speed laser melt injection, laser ablation, and electrolytic etching," J. Laser Appl. **36**(1), 012011 (2024).
[12]P. Warneke, A. Bohlen, and T. Seefeld, "Influence of the process speed in laser melt injection for reinforcing skin-pass rolls," J. Laser Appl. **35**(1), 012009 (2023).
[13]M. Picasso, C. F. Marsden, J. D. Wagniere, A. Frenk, and M. Rappaz, "A simple but realistic model for laser cladding," Metall. Mater. Trans. B **25**, 281–291 (1994).
[14]A. Bohlen and T. Seefeld, "An adaptive powder nozzle setup for enhanced efficiency in laser metal deposition," J. Laser Appl. **36**(1), 012017 (2024).
[15]S. Takemura, R. Koike, Y. Kakinuma, Y. Sato, and Y. Oda, "Design of powder nozzle for high resource efficiency in directed energy deposition based on computational fluid dynamics simulation," Int. J. Adv. Manuf. Technol. **105**(10), 4107–4121 (2019).
[16]L. Li, Y. Huang, C. Zou, and W. Tao, "Numerical study on powder stream characteristics of coaxial laser metal deposition nozzle," Crystals **11**(3), 1–13 (2021).
[17]X. X. Yao, J. Y. Li, Y. F. Wang, X. Gao, T. Li, and Z. Zhang, "Experimental and numerical studies of nozzle effect on powder flow behaviors in directed energy deposition additive manufacturing," Int. J. Mech. Sci. **210**, 106740 (2021).
[18]T. Schopphoven, "Experimentelle und modelltheoretische Untersuchungen zum Extremen Hochgeschwindigkeits-Laserauftragschweißen," Dissertation (RWTH Aachen, Aachen, 2019).
[19]G. Wang, Y. Qin, and S. Yang, "Characterization of laser-powder interaction and particle transport phenomena during laser direct deposition of W–Cu composite," Addit. Manuf. **37**, 101722 (2021).
[20]J. Volpp, H. S. Prasad, and A. Kaplan, "Behavior of heated powder particles on solid surfaces," Procedia Manuf. **25**, 365–374 (2018).
[21]K. Partes, "Hochgeschwindigkeitsbeschichten mit dem Laserstrahl," Dissertation (Universität Bremen, Bremen, 2008).
[22]HSM Stahl- und Metallhandel GmbH, Werkstoffdatenblatt 1.2362 (2023), https://www.hsm-stahl.de/wp-content/uploads/2023/07/HSM_Datenblatt_1.2362.pdf.
[23]O. Metco, "Material product data sheet spherical cast tungsten carbide powder for laser cladding," (2022), https://www.metcojoiningcladding.com/ecoma/files/DSM-0293.1_WC_LC.pdf.
[24]S. Brust, "Entwicklung abrasionsbeständiger Metallmatrix-Verbundwerkstoffe auf Eisenbasis mit ionisch-kovalenten Hartstoffen unter Betrachtung der Metall-Keramik-Interaktion," Dissertation (Ruhr Universität Bochum, Bochum, 2017).
[25]S. Nowotny, L.-M. Berger, and J. Spatzier, "Coatings by laser cladding," in *Comprehensive Hard Materials*, edited by V. K. Sarin, D. Mari, and L. Llanes (Elsevier, Amsterdam, 2014), Vol. 1, pp. 507–525.
[26]W. Ciernak, "Measuerments of the average flow velocity with the Pitot–Prandtl tube," Arch. Min. Sci. **48**(4), 415–424 (2003).
[27]H. Stroppe, *Physik für Studierende der Natur- und Ingenieurwissenschaften* (Carl Hanser Verlag, München, 2008), 14. auflage edition.
[28]R. J. L. Andon, J. F. Martin, and K. C. Mills, "Heat capacity and entropy of tungsten carbide," J. Chem. Thermodyn. **7**(11), 1079–1084 (1975).
[29]A. F. A. Hoadley and M. Rappaz, "A thermal model of laser cladding by powder injection," Metall. Mater. Trans. B **23**, 631–642 (1992).